UNIVERSITY OF CALIFORNIA, SAN DIEGO

Residual streaming flows in buoyancy driven cross-shore exchange

A thesis submitted in partial satisfaction of the
requirements for the degree
Master of Science

in

Engineering Sciences (Mechanical Engineering)

by

Ricardo Felez

Committee in charge:

Professor Antonio L. Sanchez, Co-Chair
Professor Eugene Pawlak, Co-Chair
Professor Stefan Llewellyn Smith

2017

The thesis of Ricardo Felez is approved, and it is acceptable in quality and form for publication on microfilm:

_____

_____
Co-Chair

_____
Co-Chair

University of California, San Diego

2017

DEDICATION

To my parents, for always being there.

To my grandfather, for always believing in me.

EPIGRAPH

"There is a driving force more powerful than steam, electricity and nuclear power: the will." Albert Einstein

TABLE OF CONTENTS

LIST OF FIGURES

ACKNOWLEDGEMENTS

To my advisors, Prof. Sanchez and Prof. Pawlak, for orientating me and helping me to take this project forward. They have introduced me to this exciting field of science. Thank you for their dedicated advice, encouragement and continuous support throughout my master. Their integral view on research and their mission for providing high-quality work, has made a deep impression on me. I have learnt extensively from them, including how to raise new possibilities and how to approach a problem by systematic thinking.

To my friend Victor Gandarillas, for helping me editing this project and being like a brother to me.

To my family and friends who have supported and trusted me throughout my life. Thanks to the values of perseverance and hard work that you taught me, I have come so far.

To Susan and Bill, for being like parents to me, giving me their advice and help when I most needed it.

And a special acknowledgement to my grandfather, Antonio, who passed away three years ago. Thanks to him, I had the strength to get through the hardest moments. And knowing that he would be proud of reading this project, made every minute working in this project, worth it.

ABSTRACT OF THE THESIS

Residual streaming flows in buoyancy driven cross-shore exchange

by

Ricardo Felez
Master of Science in Engineering Sciences (Mechanical Engineering)

University of California San Diego, 2017

Professor Antonio L. Sanchez, Co-Chair
Professor Eugene Pawlak, Co-Chair

Cross-shore exchange processes are of critical importance for coastal ecosystems such as coral reefs with implications for transport of nutrients, larvae and heat. We present an analytical study of two-dimensional flow in a wedge driven by a time-dependent surface heat flux as a model problem to understand buoyancy-induced cross-shore flow. Besides the turbulent Prandtl number and the Rayleigh number, both assumed to be of order unity, the solution is seen to depend on the geometry through a small parameter β measuring the bottom slope. Following previous efforts (e.g. [1]) an analytic solution is sought in the asymptotic limit $\beta \ll 1$ for a water layer bounded by an adiabatic bottom surface subject to a harmonic heat flux on the upper surface. The analysis reveals that the motion at leading order can be expressed as the sum of a harmonic component and a steady component, the latter driven by the nonlinear advection terms. This steady-streaming motion includes a nearshore and alongshore oriented vortex with associated counterclockwise recirculating motion that could have a significant effect on the near-short transport dynamics.

Chapter 1

Introduction

Cross-shore transport plays a significant role in the allocation and redistribution of heat, nutrients, sediment and pollutants across the continental shelf and the surf zone. These cross-shore exchange processes can be driven by different mechanisms, such as Ekman transport (e.g. [2]), buoyancy driven flows (e.g. [1]) or surface or internal waves (e.g. [3]). These different mechanisms become more important depending on the local characteristics, like bathymetry or stratification [4].

The field studies have shown that the contribution of the diurnal surface heat flux plays an important role in the driving mechanism of these cross-shore flows [5]. The shallower waters subjected to a surface heat flux absorb and release the heat faster than the deeper waters subjected to the same flux, this cause a baroclinic cross-shore flow that exchanges heat and momentum with the adjoining ocean. The forcing that drives this flow has a period of a day, where the heating/cooling phases each last 12 hours. The motion corresponding to the heating phase is characterized by a colder onshore flow compensated by a warmer offshore flow at the bottom. Then the flow reverses to the opposite flow corresponding to the cooling phase.

Theoretical studies have been focused on studying the thermally driven baroclinic exchange as an important mechanism in driving these flows in agreement

with field observations [6] of both, the velocity and temperature fields, at Kilo Nalu Observatory in Oahu, Hawaii.

The initial models to characterize these flows [7] considered a two dimensional domain with a rectangular cross-section. However, more recent efforts (Farrow & Patterson, [1], [8]) have used a more realistic model, where the fluid domain is contained in a infinite triangular domain. In these studies, the diurnal heating cycle is modeled as a internal heat source. The difference between the approaches by Farrow & Patterson, [1] and [8], relies on the treatment of the boundary conditions and the nature of the source. Farrow & Patterson [1] considered a periodic source term independent of the depth, with adiabatic upper and lower surfaces. However in [8] they considered a source term given by Beer's law (this term is horizontally uniform); this paper consider the bottom as a black surface (the absorbed heat is immediately released), therefore as a source, and the upper surface is adiabatic (the heat adsorbed by the upper surface is small compared to the source term).

The theoretical studies of cross-shore exchange processes can be divided in two groups, a numerical approach and an analytical approach. The analytical studies consider the slope as a small parameter to perform an expansion around it, because with the expansion, a linear system of equations is obtained and can solved to obtain the analytical expression for the temperature and velocity. Farrow and Patterson [1], found a temperature distribution that was independent of the depth, where the approximation is only appropriate close to the tip. Even though the main focus of these studies is to characterize the flow analytically, they also perform a numerical simulation to study the validity of the solution.

The numerical efforts share the same geometric model of near-shore buoyancy driven flows ([9]; [10], [11] ; [12], [13], [14]) and similarly to the analytical studies the difference relies on the definition of the boundary conditions and the source term. The geometry consists of a triangular shape wedge with a wall located at a certain distance from the tip. Lei & Patterson [10], [15] considered a similar

model to the one used by Farrow [8] (source term given by the Beer's law with a reflective bottom surface and an adiabatic upper surface). Other studies, like Mao [13], considered that the forcing term comes to play through the boundary condition in the upper surface (constant heat source) and not through an internal heat source term. The aim of these studies is to characterize all the instabilities for the different kinds of flow (e.g. viscous, laminar)

The present study is aimed at characterizing analytically the transient response of the turbid flow in a two-dimensional wedge which is subjected to a time-dependent surface heat flux. This study uses more appropriate parameters in the dimensional analysis for the turbulent flow as the ones done before (e.g. Farrow [8]) that corresponds to a natural convection flow as this analysis takes into account turbulent thermal diffusivity and viscosity.

Chapter 2

Problem formulation

Consider a two dimensional flow induced in a wedge fluid domain (Figure 2.1) of angle β with non-slip at the bottom and rigid lid in the top (where perturbations of the free surface are assumed to be small relative to the local depth). The bottom is considered to slowly vary as a function of the distance to shore. The local depth is given by:

$$z_b = -z_c h(x/x_c) \tag{2.1}$$

where z_c is the characteristic depth and x_c is the characteristic distance to shore. As the bottom does vary slowly, the angle β is chosen to be the mean slope of the bottom.

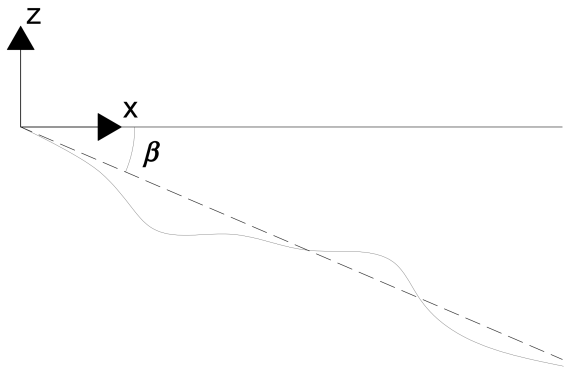

Figure 2.1: Geometry of the domain

A periodic heat flux is applied to the upper surface ($z = 0$ defined for $x > 0$), with an angular frequency ω, when $t = 0$ the heat flux is on the peak of the heating phase corresponding to midday. In this model the case of turbid water is considered, that implies that the attenuation coefficient is higher than previous efforts, where clean water was considered. This value of the attenuation coefficient implies that during the heating phase, the heat that gets to the bottom can be neglected compared with the period heat flux, therefore the bottom is assumed to be adiabatic. The surface heat flux is an appropriate approach for the cooling phase because all the heat lost is through the upper surface.

Turbulent mixing is described with an eddy turbulent viscosity, which considered here as a constant.

2.1 Governing equations

The temperature of the water increases and decreases as a consequence of the flux with a period of one day, which produces a pressure gradient that, in turn, drives a flow. These changes in temperature and the subsequent flow are governed by the Navier-Stokes equations and the energy conservation equation under the Boussinessq assumptions:

$$\frac{\partial u}{\partial x} + \frac{\partial w}{\partial z} = 0 \tag{2.2}$$

$$\frac{\partial u}{\partial t} + \frac{\partial u^2}{\partial x} + \frac{\partial wu}{\partial z} = -\frac{\partial(\frac{p'}{\rho})}{\partial x} + \nu_t \left(\frac{\partial^2 u}{\partial z^2} + \frac{\partial^2 u}{\partial x^2} \right) \tag{2.3}$$

$$\frac{\partial w}{\partial t} + \frac{\partial uw}{\partial x} + \frac{\partial w^2}{\partial z} = \left(-\frac{\partial(\frac{p'}{\rho})}{\partial z} + g\alpha(T - T_0) \right) + \nu_t \left(\frac{\partial^2 w}{\partial z^2} + \frac{\partial^2 w}{\partial x^2} \right) \tag{2.4}$$

$$\frac{\partial T}{\partial t} + \frac{\partial uT}{\partial x} + \frac{\partial wT}{\partial z} = \kappa_t \left(\frac{\partial^2 T}{\partial z^2} + \frac{\partial^2 T}{\partial x^2} \right) \tag{2.5}$$

where x and z are the horizontal and vertical coordinates respectively, with the origin located at the tip (see Figure 2.1). The horizontal velocity is indicated as u and the vertical component is given by w. P' is the pressure, T is the

temperature, ρ is the density, t is the time, g is the acceleration due to gravity, α is the thermal conductivity, ν_t is the turbulent viscosity and κ_t is the turbulent thermal diffusivity. Note that it is assumed that there are no variations in the along-shore direction (y).

The previous assumptions lead to the following boundary conditions:

- At $z = 0$:

$$\frac{\partial u}{\partial z} = w = 0 \tag{2.6}$$

$$\kappa_t \frac{\partial T}{\partial z} = \frac{q}{\rho\, C_p} cos(\omega t) \tag{2.7}$$

- At $z = z_b$:

$$\frac{\partial T}{\partial z} - \frac{\partial T}{\partial x}\frac{\partial z_b}{\partial x} = w = u = 0 \tag{2.8}$$

Where z_b is the local depth and ω is the angular frequency.

2.2 Dimensional analysis

Here we develop the analytical model in nondimensional form. From the energy equation, assuming a balance between the turbulent transport term and the variation of the temperature in time, a characteristic thickness (thickness of the heated layer) is obtained:

$$\frac{\partial T}{\partial t} \sim \kappa_t \frac{\partial^2 T}{\partial z^2} \Rightarrow \delta = \sqrt{\frac{\kappa_t}{\omega}} \tag{2.9}$$

where the characteristic time is given by the inverse of the angular frequency (ω^{-1})

The general geometry considered in this problem imposes no natural length scale. However a vertical length can be constructed by considering the growth of the thermal boundary layer at the near-horizontal rigid bottom boundary found before:

$$z_c \sim \delta \sim \sqrt{\frac{\kappa_t}{\omega}} \tag{2.10}$$

$$x_c \sim \frac{\delta}{\beta} \sim \sqrt{\frac{\kappa_t}{\omega\beta^2}} \tag{2.11}$$

From the boundary conditions for the temperature at $z = 0$, the characteristic increment of temperature is obtained as follows:

$$\kappa_t \frac{\partial T}{\partial z} \sim \frac{q}{\rho\, C_p} cos(\omega t) \Rightarrow \Delta T = \frac{(\frac{q}{\rho\, C_p})}{\sqrt{\kappa_t \omega}} \tag{2.12}$$

From the equation of the conservation of momentum in the z axis, the pressure scaling can be obtained as:

$$\frac{\partial(\frac{p'}{\rho})}{\partial z} \sim g\alpha(T - T_0) \Rightarrow \frac{p'}{\rho} = g\alpha\Delta T\delta \Rightarrow \tag{2.13}$$

$$p'_c = \frac{g\alpha q}{C_p\, \omega} \tag{2.14}$$

The characteristic velocity scales for each component can be obtained from the balance between the acceleration term and pressure gradient in the equation of conservation of momentum along the z axis:

$$\frac{\partial u}{\partial t} \sim \frac{\partial}{\partial x}\left(\frac{p'}{\rho}\right) \Rightarrow \tag{2.15}$$

$$\Rightarrow u_c = \frac{g\alpha q\beta}{\rho\, C_p \sqrt{\omega^3 \kappa_t}} \tag{2.16}$$

$$\Rightarrow w_c = \frac{g\alpha q\beta^2}{\rho\, C_p \sqrt{\omega^3 \kappa_t}} \tag{2.17}$$

The governing equations can be now expressed in dimensionless form:

$$\frac{\partial u}{\partial x} + \frac{\partial w}{\partial z} = 0 \tag{2.18}$$

$$\frac{\partial u}{\partial \tau} + Ra\ \beta^2 \left(\frac{\partial u^2}{\partial x} + \frac{\partial wu}{\partial z}\right) = -\frac{\partial p}{\partial x} + Pr\left(\frac{\partial^2 u}{\partial z^2} + \beta^2 \frac{\partial^2 u}{\partial x^2}\right) \tag{2.19}$$

$$\frac{\partial w}{\partial \tau} + Ra\,\beta^2\left(\frac{\partial uw}{\partial x} + \frac{\partial w^2}{\partial z}\right) = \beta^{-2}\left(-\frac{\partial p}{\partial z} + \theta\right) + Pr\left(\frac{\partial^2 w}{\partial z^2} + \beta^2\frac{\partial^2 w}{\partial x^2}\right) \tag{2.20}$$

$$\frac{\partial \theta}{\partial \tau} + Ra\,\beta^2\left(\frac{\partial u\theta}{\partial x} + \frac{\partial w\theta}{\partial z}\right) = \left(\frac{\partial^2 \theta}{\partial z^2} + \beta^2\frac{\partial^2 \theta}{\partial x^2}\right) \tag{2.21}$$

Where $p = \frac{p'}{\rho}$ and $\theta = \frac{T-T_0}{\Delta T}$

The Rayleigh and Prandtl number are defined as:

$$Ra = \frac{g\alpha q}{\rho C_p \omega^2 \kappa_t}, \qquad\qquad Pr = \frac{\nu_T}{\kappa_t}.$$

The boundary conditions written in dimensionless form are:

- At $z = 0$:

$$\frac{\partial u}{\partial z} = w = 0 \tag{2.22}$$

$$\frac{\partial \theta}{\partial z} = cos(\omega t) \tag{2.23}$$

- At $z = z_b$:

$$\frac{\partial \theta}{\partial z} - \beta^2\frac{\partial \theta}{\partial x}\frac{\partial z_b}{\partial x} = w = u = 0 \tag{2.24}$$

Additionally as $x \to \infty$ the fluid is at rest

$$u = w = 0, \tag{2.25}$$

and the temperature distribution is independent of x

$$\theta = \theta(z) = \frac{1}{\sqrt{2}}\,e^{-\frac{z}{\sqrt{2}}}\,cos\left(\tau - \frac{z}{\sqrt{2}} + \frac{3}{4}\pi\right) \tag{2.26}$$

Also note that from direct integration of the continuity equation (2.18), we can obtain an integral condition that must be satisfied by the solution to (2.18 − 2.24):

$$w = \int \frac{\partial u}{\partial x}\,\mathrm{d}z \Rightarrow \frac{\partial}{\partial x}\int_{z_b}^{0} u\,\mathrm{d}z = 0 \Rightarrow \int_{z_b}^{0} u\,\mathrm{d}z = 0 \tag{2.27}$$

The problem defined in (2.18−2.24) can be solved using the stream function, however in this project the problem has been solved using primitive variables.

2.3 Asymptotic solution

An asymptotic solution is obtained below for small β in the distinguished limit $Pr \sim 1$ and $Ra \sim 1$. At leading-order in the description for $\beta \ll 1$ the problem becomes linear, as is clear from inspection of (2.17)-(2.20). An interesting feature of the associated periodic solution is that, besides harmonic temperature and velocity fields, resulting from the harmonic forcing through the surface heat flux, the leading-order solution exhibits a steady component, including a residual temperature increase and associated steady-streaming velocity. The existence of this nonzero steady solution, additional to the expected harmonic response, can be anticipated by taking the time average $\langle\cdot\rangle = \frac{1}{2\pi}\int_0^{2\pi}\cdot\mathrm{d}t$ of (2.20) to yield:

$$\beta^2 Ra\left(\frac{\partial\langle u\theta\rangle}{\partial x} + \frac{\partial\langle w\theta\rangle}{\partial z}\right) = \beta^2\frac{\partial^2\langle\theta\rangle}{\partial x^2} + \frac{\partial^2\langle\theta\rangle}{\partial z^2}. \tag{2.28}$$

Integrating in z across the fluid layer with account taken of the boundary conditions given in (2.21)-(2.23) provides:

$$\frac{\partial}{\partial x}\left(Ra\int_{z_b}^{0}\langle u\theta\rangle\mathrm{d}z - \int_{z_b}^{0}\frac{\partial\langle\theta\rangle}{\partial x}\mathrm{d}z\right) = 0, \tag{2.29}$$

which further reduces to:

$$\int_{z_b}^{0} \left(Ra\langle u\theta \rangle - \frac{\partial \langle \theta \rangle}{\partial x} \right) \mathrm{d}z = 0 \tag{2.30}$$

The above exact result, independent of β, indicates that, since the product of two harmonic functions in general does not average to zero, the average temperature must also be nonzero, which in turn induces an average motion with $\langle u \rangle \neq 0$ and $\langle w \rangle \neq 0$.

As mentioned before, if β is considered as a small parameter ($\beta \ll 1$), an expansion similar to Farrow [1] can be done as follows:

$$u = u_0 + \beta^2 u_1 + \beta^4 u_2 + \ldots \tag{2.31}$$

$$w = w_0 + \beta^2 w_1 + \beta^4 w_2 + \ldots \tag{2.32}$$

$$p = p_0 + \beta^2 p_1 + \beta^4 p_2 + \ldots \tag{2.33}$$

$$\theta = \theta_0 + \beta^2 \theta_1 + \beta^4 \theta_2 + \ldots \tag{2.34}$$

Using this expansion in equations (2.18−2.21) and retaining only zero order term, the system of equations yield in a linear system of equations given by:

$$\frac{\partial u_0}{\partial x} + \frac{\partial w_0}{\partial z} = 0 \tag{2.35}$$

$$\frac{\partial u_0}{\partial \tau} = -\frac{\partial p_0}{\partial x} + Pr \frac{\partial^2 u_0}{\partial z^2} \tag{2.36}$$

$$0 = -\frac{\partial p_0}{\partial z} + \theta_0 \tag{2.37}$$

$$\frac{\partial \theta_0}{\partial \tau} = \frac{\partial^2 \theta_0}{\partial z^2} \tag{2.38}$$

with the following boundary conditions:

- At $z = 0$:

$$\frac{\partial u_0}{\partial z} = w_0 = \frac{\partial \theta_0}{\partial z} - cos(\tau) = 0 \tag{2.39}$$

- At $z = z_b$:

$$\frac{\partial \theta_0}{\partial z} = w_0 = u_0 = 0 \tag{2.40}$$

The complete solution for the leading order terms, u_0, w_0, p_0 and θ_0, can be decomposed in two contributions, one harmonic part, that carries out the time dependence, and one steady contribution.

$$u_0 = \mathbb{R}\left\{U_0(x,z)\, e^{i\tau}\right\} + \langle u_0 \rangle \tag{2.41}$$

$$w_0 = \mathbb{R}\left\{W_0(x,z)\, e^{i\tau}\right\} + \langle w_0 \rangle \tag{2.42}$$

$$p_0 = \mathbb{R}\left\{P_0(x,z)\, e^{i\tau}\right\} + \langle p_0 \rangle \tag{2.43}$$

$$\theta_0 = \mathbb{R}\left\{\Theta_0(x,z)\, e^{i\tau}\right\} + \langle \theta_0 \rangle \tag{2.44}$$

As shown above, the harmonic component of the solution is solved using separation of variables which eliminates the dependence on time and yields the following relations for the complex amplitudes:

$$\frac{\partial U_0}{\partial x} + \frac{\partial W_0}{\partial z} = 0 \tag{2.45}$$

$$iU_0 = -\frac{\partial P_0}{\partial x} + Pr\frac{\partial^2 U_0}{\partial z^2} \tag{2.46}$$

$$0 = -\frac{\partial P_0}{\partial z} + \Theta_0 \tag{2.47}$$

$$i\Theta_0 = \frac{\partial^2 \Theta_0}{\partial z^2} \tag{2.48}$$

With the boundary conditions:

- At $z = 0$:

$$\frac{\partial U_0}{\partial z} = W_0 = \frac{\partial \Theta_0}{\partial z} - 1 = 0 \tag{2.49}$$

- At $z = z_b$:

$$\frac{\partial \Theta_0}{\partial z} = W_0 = U_0 = 0 \tag{2.50}$$

The time independent Navier-Stokes equations and the heat equation are given by:

$$\frac{\partial \langle u_0 \rangle}{\partial x} + \frac{\partial \langle w_0 \rangle}{\partial z} = 0 \tag{2.51}$$

$$0 = -\frac{\partial \langle p_0 \rangle}{\partial x} + Pr \frac{\partial^2 \langle u_0 \rangle}{\partial z^2} \tag{2.52}$$

$$0 = -\frac{\partial \langle p_0 \rangle}{\partial z} + \langle \theta_0 \rangle \tag{2.53}$$

$$0 = \frac{\partial^2 \langle \theta_0 \rangle}{\partial z^2} \tag{2.54}$$

As the solution has to be independent of time, the boundary conditions become:

- At $z = 0$:

$$\frac{\partial \langle u_0 \rangle}{\partial z} = \langle w_0 \rangle = \frac{\partial \langle \theta_0 \rangle}{\partial z} = 0 \tag{2.55}$$

- At $z = -\beta x$:

$$\frac{\partial \langle \theta_0 \rangle}{\partial z} = \langle w_0 \rangle = \langle u_0 \rangle = 0 \tag{2.56}$$

The harmonic problem, equations $(2.45 - 2.50)$, is solved in Chapter 3 and the steady problem, equations $(2.51 - 2.56)$, is solved in Chapter 4. To finalize in Chapter 5, the complete solution is analyzed.

Chapter 3

Harmonic solution

The set of equations given in $(2.45 - 2.48)$ are solved in this chapter.

3.1 Analytical solution

From (2.48), the temperature can be obtained easily:

$$\Theta_0 = C_1(x)e^{\frac{i+i}{\sqrt{2}}z} + C_2(x)e^{-\frac{i+i}{\sqrt{2}}z} \tag{3.1}$$

After applying the boundary conditions, $\frac{\partial \Theta_0}{\partial z}\big|_{z=0} - 1 = \frac{\partial \Theta_0}{\partial z}\big|_{z=z_b} = 0$, the zero order temperature Θ_0 is:

$$\Theta_0 = -\frac{(1-i)}{\sqrt{2}} \frac{\left(e^{-\frac{1+i}{\sqrt{2}}(z-2z_b)} + e^{\frac{1+i}{\sqrt{2}}z}\right)}{\left(e^{2\frac{1+i}{\sqrt{2}}z_b} - 1\right)} \tag{3.2}$$

$$\tilde{\theta}_0 = \mathbb{R}\left\{\Theta_0\, e^{i\tau}\right\}$$

The main balance as $\beta \to 0$ is between the unsteady term and the diffusion term. The temperature distribution is independent of the Prandtl number. Unlike the zero order temperature distribution obtained by Farrow [1], the distribution found in this study is dependent on the depth. It is easy to check that this

temperature distribution is also consistent with field observations ([4]), where, as $x \to 0$, the temperature increment/decrement is higher.

If we take the partial derivative of (2.47) with respect to x and the partial derivative of (2.46) with respect to z, we eliminate the pressure, and equation (2.46) becomes:

$$i\frac{\partial U_0}{\partial z} = -\frac{\partial \Theta_0}{\partial x} + Pr\frac{\partial^3 U_0}{\partial z^3} \tag{3.3}$$

The solution for the equation (2.46) can be decomposed into two parts, a particular solution plus a homogeneous solution:

$$U_0 = U_{0,part} + U_{0,hom}$$

The expression for the particular solution is given by:

$$U_{0,part} = 2\,\frac{1+i}{\sqrt{2}}\,\frac{\left(e^{2\frac{1+i}{\sqrt{2}}z} - 1\right)e^{-\frac{1+i}{\sqrt{2}}(z-2z_b)}}{(1-Pr)\left(e^{2\frac{1+i}{\sqrt{2}}z_b} - 1\right)^2}\,\frac{d\,z_b}{dx} \tag{3.4}$$

As can be seen, the previous expression has a singularity when the value of the Prandtl number is equal to one, however the velocity has to be finite for all the values of the Prandtl number. The particular solution for $Pr = 1$ can be then found in the limit $Pr \to 1$.

$$
\begin{aligned}
&U_{0,part}\Big|_{Pr=1} = \lim_{Pr\to 1} U_{0,part} = \\
&= -\frac{\left(\frac{1}{4}+\frac{i}{4}\right) e^{-\frac{1+i}{\sqrt{2}}\ z}}{\left(e^{2\frac{1+i}{\sqrt{2}}\ z_b}-1\right)^2}\left[\left((2+2i)(z-1)-3\sqrt{2}+\sqrt{2}e^{-2\frac{1+i}{\sqrt{2}}}\right)e^{2\frac{1+i}{\sqrt{2}}\ (z_b+z)}\right]\frac{d\,z_b}{dx}- \\
&-\frac{\left(\frac{1}{4}+\frac{i}{4}\right) e^{-\frac{1+i}{\sqrt{2}}\ z}}{\left(e^{2\frac{1+i}{\sqrt{2}}\ z_b}-1\right)^2}\left[\left(3\sqrt{2}+(2+2i)z\right)e^{2\frac{1+i}{\sqrt{2}}\ z_b}\right]\ \frac{d\,z_b}{dx}
\end{aligned}
\tag{3.5}
$$

The homogeneous equation for the horizontal velocity can be treated as a linear ODE with constant coefficients, yielding the solution:

$$
U_{0,hom} = -\frac{1+i}{\sqrt{2}}\sqrt{Pr}\ e^{-\frac{1+i}{\sqrt{2Pr}}\ z}\left(C_2(x) - C_1(x)\ e^{2\frac{1+i}{\sqrt{2Pr}}\ z}\right) + C_3(x). \tag{3.6}
$$

The expression of the coefficients $C_1(x)$, $C_2(x)$, and $C_3(x)$ are shown in Appendix 1. This coefficients can be interpreted as constants of integration with with respect to z. These are found by proper application of the boundary conditions, $\frac{\partial U_0}{\partial z}\big|_{z=0} = U_0\big|_{z=z_b(x)} = 0$ and the additional integral condition given in (2.27), that particularize for the harmonic solution becomes: $\int_{z_b}^{0} U_0\ \mathrm{d}z = 0$.

Once the horizontal component of the velocity is obtained, the vertical velocity can be calculated using the continuity equation (2.45). The solution of the vertical component of the velocity can be decomposed as a particular solution and a homogeneous one in a similar manner to the horizontal component.

$$
W_0 = \int_0^z \frac{\partial U_0}{\partial x}dz = \int_0^z \frac{\partial U_{0,part}}{\partial x}dz + \int_0^z \frac{\partial U_{0,hom}}{\partial x} = W_{0,part} + W_{0,hom} \tag{3.7}
$$

The expression of the particular solution is:

$$
W_{0,part} = \frac{2\left(e^{\frac{1+i}{\sqrt{2}}\ z}-1\right)^2 e^{-\frac{1+i}{\sqrt{2}}\ (z-2z_b)}\left(2\sqrt[4]{-1}\left(e^{2\frac{1+i}{\sqrt{2}}\ z_b}+1\right)\left(\frac{d\,z_b}{dx}\right)^2-\left(e^{2\frac{1+i}{\sqrt{2}}\ z_b}-1\right)\frac{d^2 z_b}{dx^2}\right)}{(Pr-1)\left(e^{2\frac{1+i}{\sqrt{2}}\ z_b}-1\right)^3} \tag{3.8}
$$

The expression of the particular solution for horizontal velocity has a singularity as $Pr \to 1$, so does the particular solution for the vertical velocity. The problem can be solved in a similar way.

$$W_{0,part}\Big|_{Pr=1} = \lim_{Pr\to 1} W_{0,part} \tag{3.9}$$

The homogeneous part is given by:

$$W_{0,hom} = zC_3'(x) - iPr\left[\left(e^{\frac{1+i}{\sqrt{2Pr}}z} - 1\right)C_1'(x) + \left(e^{-\frac{1+i}{\sqrt{2Pr}}z} - 1\right)C_2'(x)\right] \tag{3.10}$$

3.2 Discussion of the harmonic solution

In this treatment, the local depth is considered as a function of the distance to shore. We consider a bottom boundary that has small variations with respect to the mean slope, so that it can be approximated as $z_b = -x$.

As mentioned before, the temperature profile depends on the depth. Away from shore, the ratio of the height of the heated layer to the local depth decreases. In other words, as the distance to shore increases, the effects of the surface heat flux are contained to a layer that is thin relative to the depth as shown in Figure 3.1. This phenomenon can be seen in Figure 3.1. Figure 3.1 also shows that the shallower regions absorb more heat than the deeper regions, in agreement with the field observations .

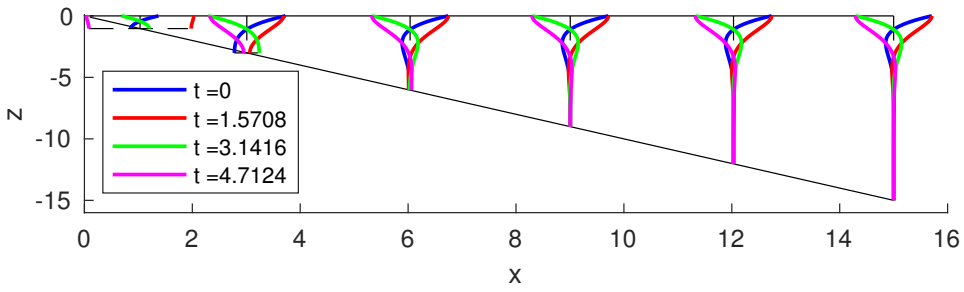

Figure 3.1: Temperature profiles at $x = 1, 3, 6, 9, 12$ and 15 for different times

In contrast to Farrow [1], where the streamlines go to infinity and a vortex is formed when the flow reverses, in the case of turbid water and periodic heat flux on the surface, the

velocity field has multiple vortices where the intensity of the vortices decays with the distance to shore. This is shown clearly in Figure 3.2, where the streamlines are plotted for different times. Looking at Figure 3.2 it is apparent that the vortices move off-shore becoming bigger and weaker over time. In what follows, a thorough discussion of the velocity field with $Pr = 1$ is provided for clarity before addressing the influence of the Prandtl number on the velocity field.

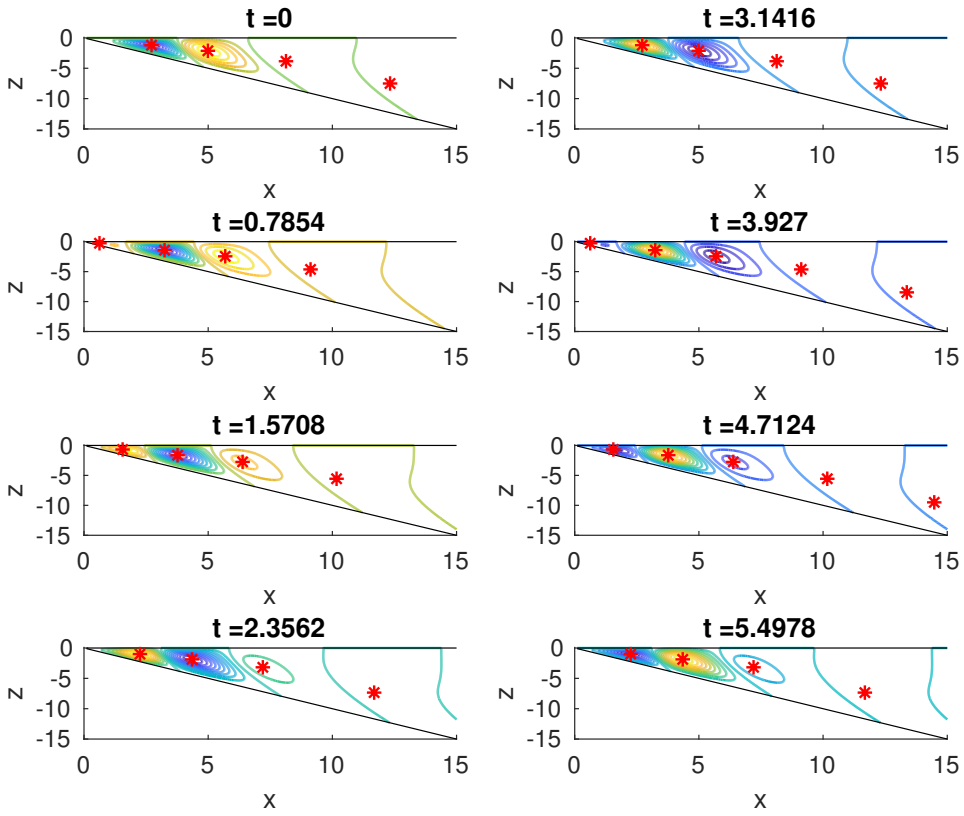

Figure 3.2: Streamlines at different times for $Pr = 1$. The asterisks denote the position of the vortex peak.

The velocity field can be divided into two regions: the viscous region ($x \to 0$), where the main balance is between the viscous terms and the horizontal pressure gradient, and the inertial region, where viscosity can be neglected and the main balance is between the inertia terms and the horizontal pressure gradient. The behavior of the flow in the viscous region is characterized by an immediate adaptation to the changes in the forcing, as is shown in Figure 3.3 (right).

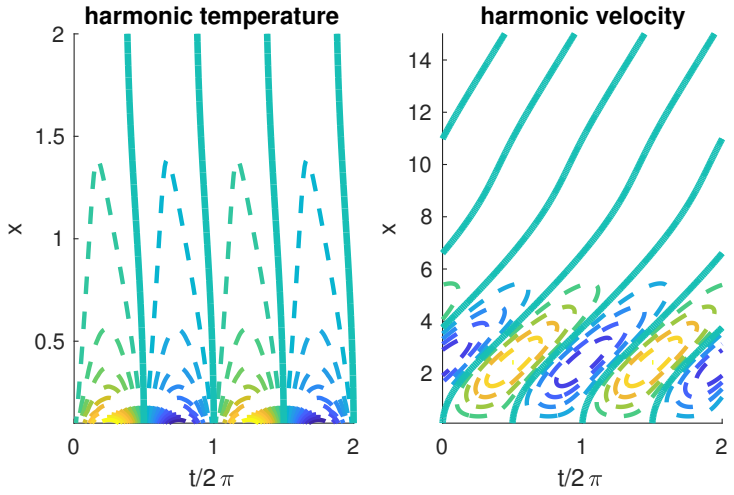

Figure 3.3: Contours of the surface temperature and velocity in the (t-x) plane

In Figure 3.3, the contours of surface temperature ($\theta_0|_{z=0}$) and velocity ($u_0|_{z=0}$) are plotted as a function of the time (expressed as a the number of cycles). The surface temperature plot shows the phenomenon mentioned before, the temperature ranges is higher in the shallower regions is higher than in the deeper regions. When $t = n/2$ ($n = 0, 1, 2, ...$), a reversal of the force leads to a creation of a new vortex. In both plots, the solid contours represent the stagnation point ($u_0|_{z=0} = 0$), where the pressure gradient changes sign. In the surface velocity plot as, $x \to 0$, the flow adjusts immediately to the changes in the forcing as it corresponds to the viscous-dominated region. In both plots, the regions in which the contours are yellow represent the heating phase, for the surface velocity plot the circulation of the vortex in the heating phase is clock-wise, and the blue regions represent the cooling period, in which the circulation of the vortex is anti clock-wise.

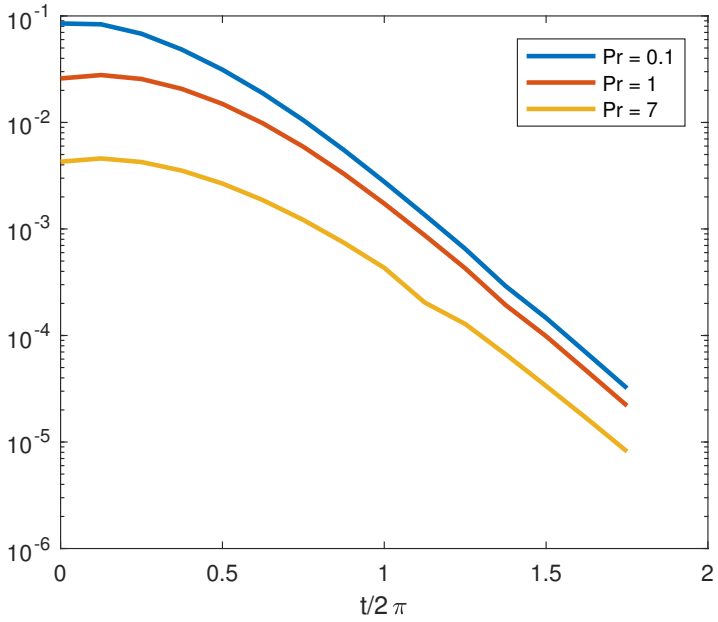

Figure 3.4: Magnitude of the vortex of the velocity for different Pr

The Prandtl number, which represents the ratio of viscosity to thermal diffusivity, influences the fluid flow as long as the temperature and velocity field are coupled, such as in the context of the Boussinesq approximation. As Pr increases, the flow will become more viscous and the magnitude of the velocity decreases, as shown in Figure 3.4. Vortex magnitudes decrease with time and also weaken with increasing Pr. It is also illuminating to look at both limits of the Prandtl number ($Pr \to 0$ and $Pr \to \infty$). As $Pr \to 0$, thermal diffusion is dominant in comparison with momentum diffusion. Viscous effects are relatively weak so that the changes in the velocity are limited to a small layer, or in other words, there is going to be two boundary layers in both boundary layers. Figure 3.5 shows that there is a boundary layer at $z = 0$ and another one when $z = z_b$. In the case of the limit of $Pr \to \infty$, the momentum diffusion is dominant compared to the thermal diffusion. In this limit the flow is so viscous that the flow does not move. Examination of this problem would require rescaling of the equations using alternate parameters.

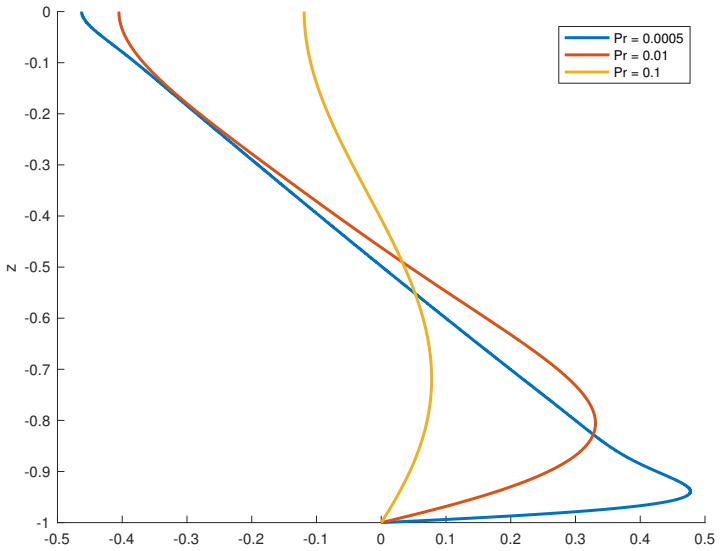

Figure 3.5: Horizontal velocity profile at $x = 1$ and $t = 0$

Chapter 4

Steady solution

The complete solution has to satisfy the equation given in (2.30). As mentioned before, if the product of two harmonic functions in general does not average to zero, the average temperature must also be nonzero, which implies that a steady solution may exist, and in fact, for the case considered in this study, a steady solution must exist, as shown below.

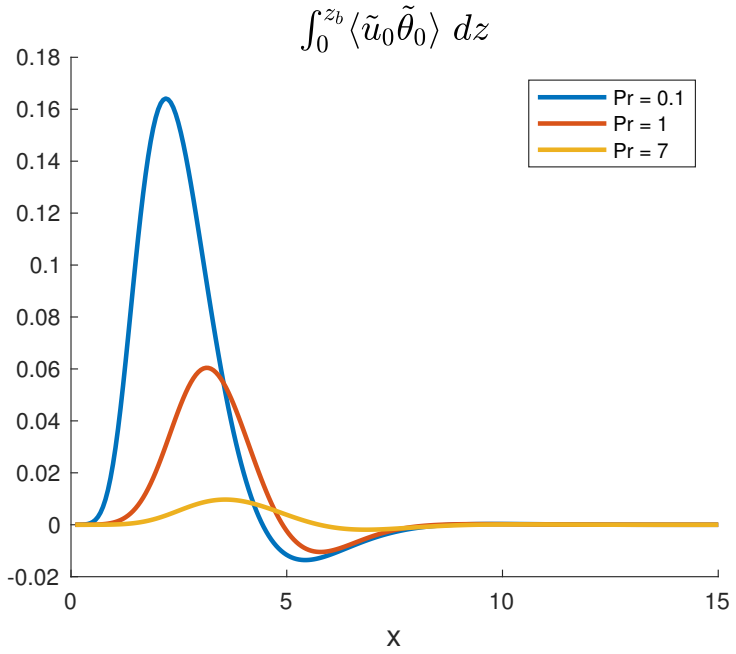

Figure 4.1: Heat flux along the boundary layer

The fact that the heat flux of the harmonic solution is not constant along the boundary

layer requires the existance of a steady solution.

4.1 Analitical solution

The expression for the temperature is trivial:

$$\langle \theta_0 \rangle = f\,(x) \tag{4.1}$$

Where $f(x)$ is a unknown function of x.

Once the temperature distribution is known, the velocity field can be calculated. The pressure can be eliminated from in a similar manner to the harmonic component. If we take the partial derivative with respect to x of (2.53) and the partial derivative with respect to z of (2.52) the pressure can be eliminated, and the equation (2.52) becomes:

$$0 = -\frac{\partial \langle \theta_0 \rangle}{\partial x} + Pr \frac{\partial^3 \langle u_0 \rangle}{\partial z^3} \tag{4.2}$$

The steady component of the horizontal velocity can be found by integrating (4.2) three times and after applying the boundary conditions, $\frac{\partial \langle u_0 \rangle}{\partial z}\Big|_{z=0} = \langle u_0 \rangle\big|_{z=z_b} = 0$ and the integral condition $\int_{z_b}^{0} \langle u_0 \rangle \mathrm{d}z = 0$, the expression for the horizontal component is given by:

$$\langle u_0 \rangle = \frac{8\,z^3 - 9\,z^2 z_b + z_b^3}{48 Pr}\; f'(x) \tag{4.3}$$

where $\cdot' = \frac{d}{dx}$

The expression of the vertical component can be found if we apply the continuity equation (2.51):

$$\langle w_0 \rangle = \int_0^z \frac{\partial \langle u_0 \rangle}{\partial x} dz = \frac{z\,z_b^2 - \,z^3}{48 Pr}\; f'(x) + \frac{3\,z^3 z_b - z\,z_b^3 - 2\,z^4}{48 Pr}\; f''(x) \tag{4.4}$$

At zero order, the solution is undetermined as both the temperature and velocity field depend of an unknown function of x and its derivatives. We can determine the function $f(x)$ we can carry the first order perturbation in the analysis or we can use the condition given in (2.30), which is exact. If the expressions $(2.41 - 2.41)$ are introduced in (2.30), (2.30) becomes:

$$\int_{z_b}^{0} \left(Ra \langle \left(\mathbb{R}\left\{ U_0\, e^{i\tau} \right\} + \langle u_0 \rangle \right) \left(\mathbb{R}\left\{ \Theta_0\, e^{i\tau} \right\} + \langle \theta_0 \rangle \right) \rangle - \frac{\partial \langle \left(\mathbb{R}\left\{ \Theta_0\, e^{i\tau} \right\} + \langle \theta_0 \rangle \right) \rangle}{\partial x} \right) \mathrm{d}z = 0 \tag{4.5}$$

The following terms of 4.5 go to zero because the average of a harmonic function is zero:

$$\int_{z_b}^{0} \langle \left(\mathbb{R}\left\{U_0\, e^{i\tau}\right\}\right) \langle \theta_0 \rangle \rangle \, \mathrm{d}z = \int_{z_b}^{0} \langle \left(\mathbb{R}\left\{\Theta_0\, e^{i\tau}\right\}\right) \langle u_0 \rangle \rangle \mathrm{d}z = \int_{z_b}^{0} \frac{\partial \langle \mathbb{R}\left\{\Theta_0\, e^{i\tau}\right\}\rangle}{\partial x} \, \mathrm{d}z = 0$$

Remembering that the steady temperature is independent of z the term of the product of the steady temperature and velocity goes to zero, as shown below:

$$\int_{z_b}^{0} \langle \theta_0 \rangle \langle u_0 \rangle \, \mathrm{d}z = \langle \theta_0 \rangle \int_{z_b}^{0} \langle u_0 \rangle \, \mathrm{d}z = 0$$

Applying this simplifications equation (4.5) yields:

$$Ra \int_{z_b}^{0} \left(\langle \left(\mathbb{R}\left\{U_0\, e^{i\tau}\right\}\right) \left(\mathbb{R}\left\{\Theta_0\, e^{i\tau}\right\}\right) \rangle - f'(x) \right) \mathrm{d}z = 0 \tag{4.6}$$

At the limit $x \to \infty$, the fluid is at rest and the temperature is independent of x, therefore the boundary condition for $f(x)$ is $f(\infty) = 0$

4.2 Discussion of the steady solution

In this approach to the cross-shore exchange problem, the analysis shows that, at leading order, there is a residual streaming flow. As mentioned before, this flow results from the requirement that heat cannot accumulate at a given x location. One of the reasons for the existence of this residual flow is that the harmonic velocity and the harmonic solution are partly out phase ($0 \leq \varphi < \pi$). In previous studies, such as Farrow [1], where the temperature distribution is independent of the depth, the flow will not have the residual flow at zero order. This can be shown as follows:

$$\frac{d}{dx} \int_0^{z_b} \langle u_0(x,z)\theta_0(x) \rangle \; dz = \frac{d}{dx} \langle \theta_0(x) \int_0^{z_b} u_0(x,z) \; dz \rangle \tag{4.7}$$

And remembering the integral condition given in (2.27):

$$\frac{d}{dx} \langle \theta_0(x) \int_0^{z_b} u_0(x,z) \; dz \rangle = 0 \tag{4.8}$$

Once the residual flow has been introduced, the temperature distribution may be analyzed. The steady temperature distribution, unlike the harmonic distribution, depends on the Prandtl number. This dependence comes from the fact that the function $f(x)$ depends on u_0, which also depends on the Prandtl number. Figure 4.2 shows how the temperature distribution varies with Pr.

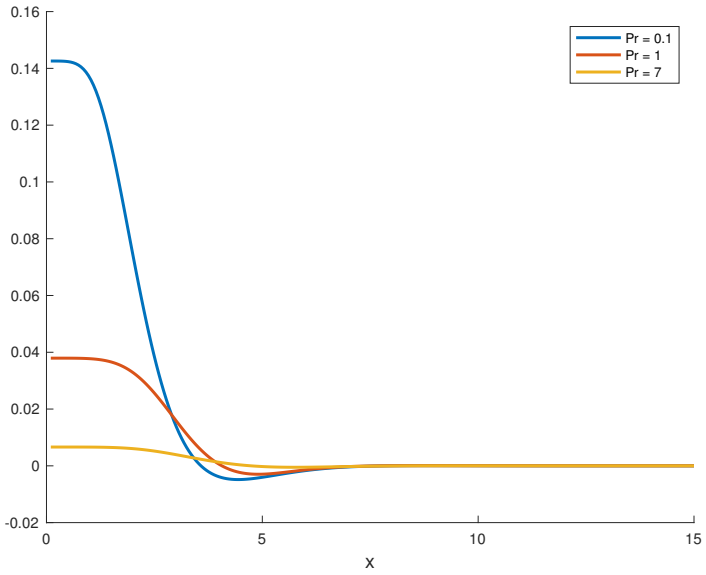

Figure 4.2: Function $f(x)$ for different values of the Prandtl number

Equation 4.6 shows that the function $f(x)$ is proportional to the Rayleigh number, therefore the steady solution for both the temperature and velocity, will be also linearly proportional to the Rayleigh number.

The velocity distribution has multiple number of vortices, as can be seen in Figure 4.3, where the streamlines have been plotted for different Prandtl numbers. These vortices become bigger and weaker as the distance to shore increases in a similar manner to the harmonic solution. The vortices also depend on the Prandtl number, as it increases, the vortices grow in size and their intensity decays. This fact can be observed as well in Figure 4.3

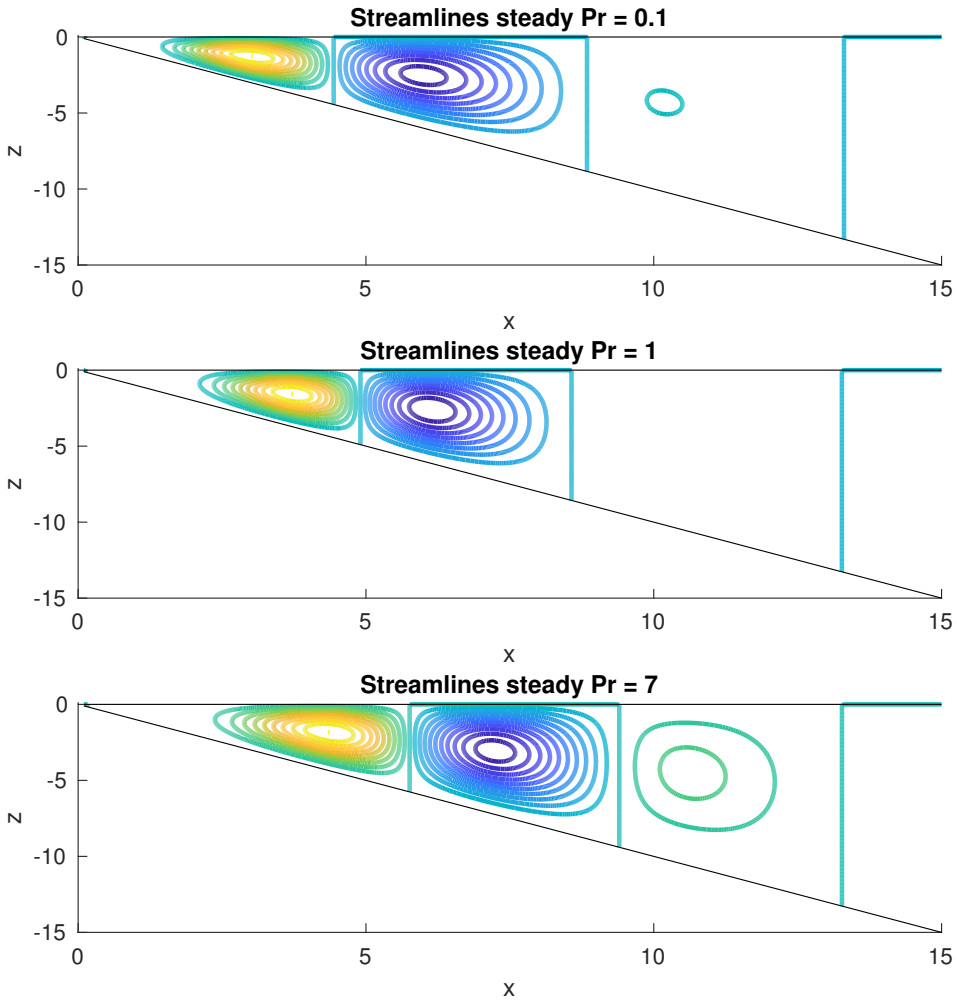

Figure 4.3: Streamlines of the steady solution for different Prandtl numbers

Chapter 5

Complete solution

The complete solution is given by the combination of the harmonic and steady components:

$$u_0 = \tilde{u}_0 + \langle u_0 \rangle$$

$$w_0 = \tilde{w}_0 + \langle w_0 \rangle$$

$$\theta_0 = \tilde{\theta}_0 + \langle \theta_0 \rangle$$

When the full solution is considered, the Rayleigh number plays an important role in the flow structure, determining the relative contributions. Figure 5.1 compares the decay ratio of the vortices of the harmonic solution and the steady solution. The Rayleigh number determines the amplitude of the steady vortex decay curve as shown in 5.1. In other words, as the Rayleigh number increases, the steady solution becomes dominant.

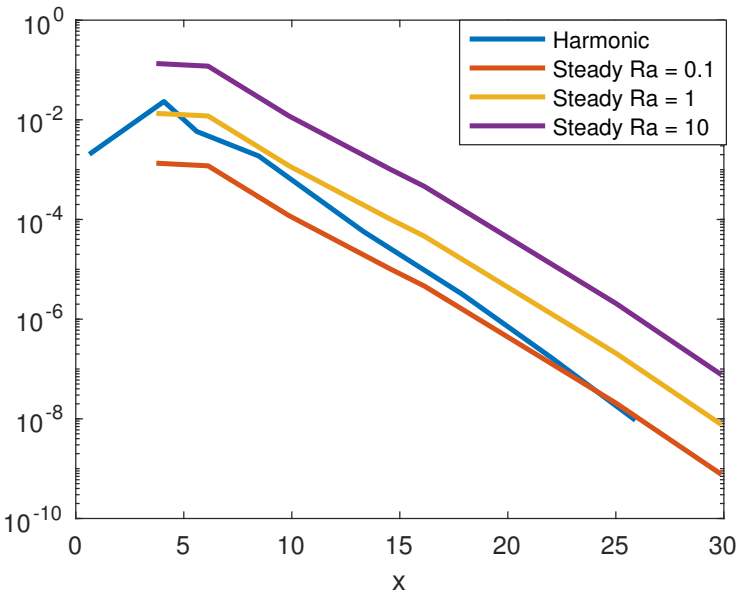

Figure 5.1: Magnitude of the vortices as x increases

Figure 5.2 shows the shape of the surface velocity with respect to time for different values of the Rayleigh number. As can be seen, when $Ra = 0.1$ if $0 \leq x \leq 6$ the harmonic solution is dominant and if $x \geq 6$ the steady solution is comparable to the harmonic solution and becomes the dominant solution. For a $Ra = 1$, the steady solution is comparable to the harmonic one in distances to shore of order one. In the case that the other limit is considered, $Ra \gg 1$ the steady solution is dominant in the whole domain except in a small region close to the tip.

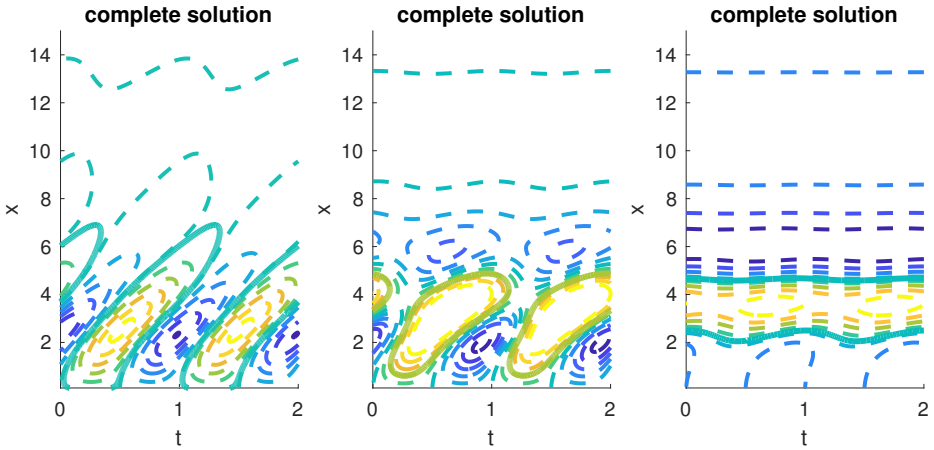

Figure 5.2: Surface velocity for $Ra = 0.1$, $Ra = 1$ and $Ra = 10$

It is of interest to analyze the behavior of the vortices in the region where both solutions

are comparable. To illustrate this analysis, the streamlines for the case of $Ra = 1$ have been plotted and can be seen in Figure 5.2. In the harmonic region the vortices travel off shore, becoming weaker as they travel. These traveling vortices are then absorbed by the steady vortices and they no longer travel, but begin to oscillate. These oscillations are shown in Figure 5.3.

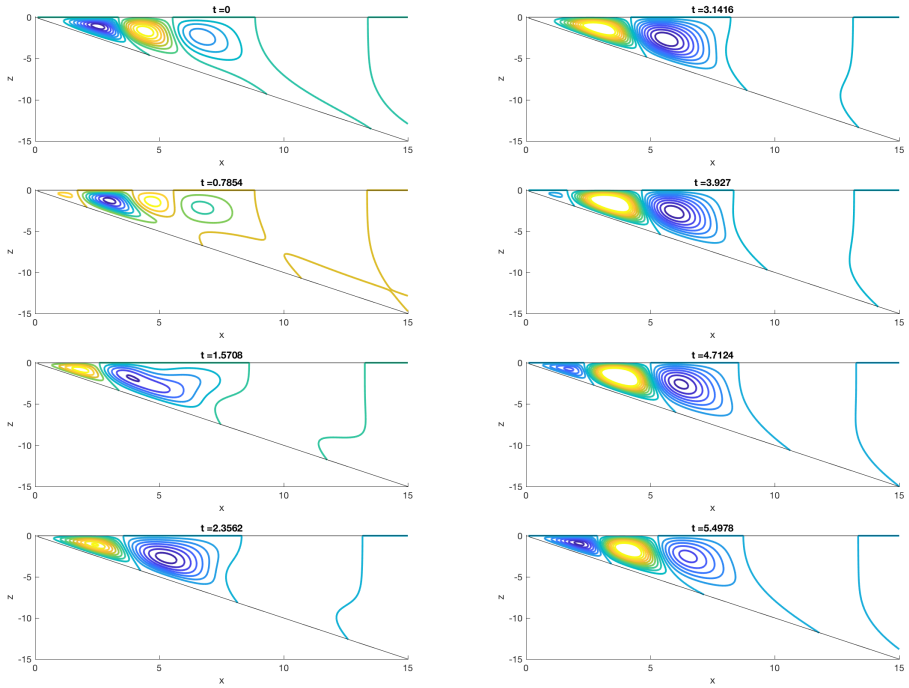

Figure 5.3: Surface velocity for $Ra = 0.1$, $Ra = 1$ and $Ra = 10$

Chapter 6

Concluding remarks

This paper presents an analytical model of turbid water flow in an infinite wedge. An asymptotic solution has been found for a particular case of the complex geophysical situation.

The results obtained from solving the unsteady Navier-Stokes equation shows that the harmonic temperature is consistent with the field studies. The absorbed/released heat flux decreases as the distance to shore increases. The harmonic solution also shows that the velocity distribution has an infinite number of traveling vortices, which intensity of these vortices decreases as they travel away from shore.

When perturbations of the first order are considered, there is an accumulation of heat in the inside of the fluid domain. A residual streaming flow appears in the leading order distribution to compensate for the accumulation of heat. The streamlines of the residual streaming flow show the presence of an infinite number of steady vortices, whose intensities decay in a similar manner as the harmonic component.

The final distribution of temperature and velocity is the sum of the harmonic and the steady contributions.

Dimensional analysis shows that the only parameters influencing velocity and temperature distribution are the Prandtl and Rayleigh number. A analysis of the influence of both parameters has been performed showing that as the Prandtl number the Prandtl number increases, the vortices become weaker and bigger. The limiting cases have also been explored. In the case where $Pr \to 0$ there are two boundary layers in both surfaces. As $Pr \to \infty$ there will be no motion and a new dimensional analysis is required.

The Rayleigh number has an important role in the final solution, making the steady

solution more or less dominant with respect to the harmonic one. If $Ra \ll 1$, the harmonic solution will be dominant in the region closer to shore. If $Ra \gg 1$ however, the steady solution will be dominant. The last case considered is when $Ra \sim 1$ both solution can be compared, the traveling vortices from the harmonic component are absorbed by the steady solution and they start to oscillate around a certain x coordinate.

Chapter 7

Appendix A

A.1. Notation

C_p	Specific heat capacity
g	Acceleration due to gravity
P'	Pressure
Pr	Prandtl number $Pr = \frac{\nu_T}{\kappa_t}$
q	Specific heat
Ra	Rayleigh number $Ra = \frac{g\alpha q}{\rho C_p \omega^2 \kappa_t}$
t	Time
T	Temperature
ΔT	Characteristic increment of temperature
u, w	Velocity components in x and y directions
u_c, w_c	Characteristic velocity in x and y directions
x, z	Coordinates in horizontal and vertical directions
x_c, z_c	Characteristic horizontal and vertical lengths
z_b	Local depth $z_b = -z_c h(x/x_c)$
Greeks	
α	Thermal conductivity
β	Bottom mean slope
δ	Characteristic thickness
ω	Angular velocity
ρ	Density
θ	Non-dimensional temperature
κ_t	Turbulent thermal diffusivity
ν_t	Turbulent viscosity

A.2. Constants of integration

Here the expresions of the terms $C_1(x)$, $C_2(x)$, $C_3(x)$, $C_1'(x)$, $C_2'(x)$ and $C_3'(x)$

$$denominator_{C_1} = 2(Pr-1)\sqrt{Pr}\left(1+\cosh\left(\frac{(1+i)\,z_b}{\sqrt{2}}\right)\right)$$
$$\left(\left(-\sqrt{Pr}+\frac{(1+i)\,z_b}{\sqrt{2}}\right)\left(\sinh\left(\frac{(1+i)\sqrt{2}\,z_b}{\sqrt{Pr}}\right)+\cosh\left(\frac{(1+i)\sqrt{2}\,z_b}{\sqrt{Pr}}\right)\right)+\sqrt{Pr}+\frac{(1+i)\,z_b}{\sqrt{2}}\right)$$

$$C_1(x) = \left[-\frac{\left[\sinh\left(\frac{(1+i)z_b}{\sqrt{2}\sqrt{Pr}}\right)+\cosh\left(\frac{(1+i)z_b}{\sqrt{2}\sqrt{Pr}}\right)\right]\left[Pr-\frac{(1+i)z_b\sinh\left(\frac{(1+i)z_b}{\sqrt{2}}\right)}{\sqrt{2}}+\cosh\left(\frac{(1+i)z_b}{\sqrt{2}}\right)-1\right]}{denominator_{C_1}}+\right.$$
$$\left.+\frac{\left[\frac{(1+i)\sqrt{Pr}z_b}{\sqrt{2}}\right]\left[Pr-\frac{(1+i)z_b\sinh\left(\frac{(1+i)z_b}{\sqrt{2}}\right)}{\sqrt{2}}+\cosh\left(\frac{(1+i)z_b}{\sqrt{2}}\right)-1\right]}{denominator_{C_1}}\right] i\,z_b'\,\mathrm{csch}^2\left(\frac{\left(\frac{1}{2}+\frac{i}{2}\right)z_b}{\sqrt{2}}\right) \tag{7.1}$$

$$C_2(x) = -\frac{2e^{\frac{\sqrt[4]{-1}(\sqrt{Pr}+1)\,z_b}{\sqrt{Pr}}}\left[(-1)^{3/4}\,z_b\left(-2\sqrt{Pr}e^{\frac{\sqrt[4]{-1}(\sqrt{Pr}+1)\,z_b}{\sqrt{Pr}}}+e^{2\sqrt[4]{-1}\,z_b}-1\right)\right]z_b'}{(Pr-1)\sqrt{Pr}\left(e^{2\sqrt[4]{-1}\,z_b}-1\right)^2\left(e^{\frac{2\sqrt[4]{-1}\,z_b}{\sqrt{Pr}}}\left(\sqrt[4]{-1}\,z_b-\sqrt{Pr}\right)+\sqrt{Pr}+\sqrt[4]{-1}\,z_b\right)}+$$
$$+\frac{2e^{\frac{\sqrt[4]{-1}(\sqrt{Pr}+1)\,z_b}{\sqrt{Pr}}}\left[i\left(e^{\sqrt[4]{-1}\,z_b}\left(-2Pr\,e^{\frac{\sqrt[4]{-1}\,z_b}{\sqrt{Pr}}}+2Pr+e^{\sqrt[4]{-1}\,z_b}-2\right)+1\right)\right]z_b'}{(Pr-1)\sqrt{Pr}\left(e^{2\sqrt[4]{-1}\,z_b}-1\right)^2\left(e^{\frac{2\sqrt[4]{-1}\,z_b}{\sqrt{Pr}}}\left(\sqrt[4]{-1}\,z_b-\sqrt{Pr}\right)+\sqrt{Pr}+\sqrt[4]{-1}\,z_b\right)} \tag{7.2}$$

$$C_3(x) = \frac{2\sqrt[4]{-1}e^{\sqrt[4]{-1}\,z_b}\left[\left(\sqrt{Pr}-1\right)\left(-e^{\frac{2\sqrt[4]{-1}(\sqrt{Pr}+1)\,z_b}{\sqrt{Pr}}}\right)+\left(\sqrt{Pr}+1\right)e^{2\sqrt[4]{-1}\,z_b}\right]z_b'}{(Pr-1)\left(e^{2\sqrt[4]{-1}\,z_b}-1\right)^2\left(e^{\frac{2\sqrt[4]{-1}\,z_b}{\sqrt{Pr}}}\left(\sqrt[4]{-1}\,z_b-\sqrt{Pr}\right)+\sqrt{Pr}+\sqrt[4]{-1}\,z_b\right)}+$$
$$+\frac{2\sqrt[4]{-1}e^{\sqrt[4]{-1}\,z_b}\left[\left(\sqrt{Pr}+1\right)e^{\frac{2\sqrt[4]{-1}\,z_b}{\sqrt{Pr}}}+2(Pr-1)e^{\sqrt[4]{-1}\,z_b}+2(Pr-1)e^{\frac{\sqrt[4]{-1}(\sqrt{Pr}+2)\,z_b}{\sqrt{Pr}}}\right]z_b'}{(Pr-1)\left(e^{2\sqrt[4]{-1}\,z_b}-1\right)^2\left(e^{\frac{2\sqrt[4]{-1}\,z_b}{\sqrt{Pr}}}\left(\sqrt[4]{-1}\,z_b-\sqrt{Pr}\right)+\sqrt{Pr}+\sqrt[4]{-1}\,z_b\right)} \tag{7.3}$$
$$-\frac{2\sqrt[4]{-1}e^{\sqrt[4]{-1}\,z_b}\left[4Pre^{\frac{\sqrt[4]{-1}(\sqrt{Pr}+1)\,z_b}{\sqrt{Pr}}}-\sqrt{Pr}+1\right]z_b'}{(Pr-1)\left(e^{2\sqrt[4]{-1}\,z_b}-1\right)^2\left(e^{\frac{2\sqrt[4]{-1}\,z_b}{\sqrt{Pr}}}\left(\sqrt[4]{-1}\,z_b-\sqrt{Pr}\right)+\sqrt{Pr}+\sqrt[4]{-1}\,z_b\right)}$$

Bibliography

[1] DE Farrow and JC Patterson. On the response of a reservoir sidearm to diurnal heating and cooling. *Journal of Fluid Mechanics*, 246:143–161, 1993.

[2] VCFDLE Combes, Fanny Chenillat, E Di Lorenzo, P Rivière, MD Ohman, and SJ Bograd. Cross-shore transport variability in the california current: Ekman upwelling vs. eddy dynamics. *Progress in Oceanography*, 109:78–89, 2013.

[3] James J Leichter, Gregory Shellenbarger, Salvatore J Genovese, and Stephen R Wing. Breaking internal waves on a florida (usa) coral reef: a plankton pump at work? *Marine Ecology Progress Series*, pages 83–97, 1998.

[4] Stephen G Monismith, Amatzia Genin, Matthew A Reidenbach, Gitai Yahel, and Jeffrey R Koseff. Thermally driven exchanges between a coral reef and the adjoining ocean. *Journal of Physical Oceanography*, 36(7):1332–1347, 2006.

[5] Stephen G Monismith, Jörg Imberger, and Michael L Morison. Convective motions in the sidearm of a small reservoir. *Limnology and Oceanography*, 35(8):1676–1702, 1990.

[6] L Molina, G Pawlak, JR Wells, SG Monismith, and MA Merrifield. Diurnal cross-shore thermal exchange on a tropical forereef. *Journal of Geophysical Research: Oceans*, 119(9):6101–6120, 2014.

[7] Adrian Bejan, Adnan A Al-Homoud, and Jorg Imberger. Experimental study of high-rayleigh-number convection in a horizontal cavity with different end temperatures. *Journal of Fluid Mechanics*, 109:283–299, 1981.

[8] DE Farrow and JC Patterson. The daytime circulation and temperature structure in a reservoir sidearm. *International Journal of Heat and Mass Transfer*, 37(13):1957–1968, 1994.

[9] Jeff J Sturman, Carolyn E Oldham, and Greg N Ivey. Steady convective exchange flows down slopes. *Aquatic Sciences*, 61(3):260, 1999.

[10] Chengwang Lei and John C Patterson. Unsteady natural convection in a triangular enclosure induced by absorption of radiation. *Journal of Fluid Mechanics*, 460:181–209, 2002.

[11] Chengwang Lei and John C Patterson. Unsteady natural convection in a triangular enclosure induced by surface cooling. *International Journal of Heat and Fluid Flow*, 26(2):307–321, 2005.

[12] Yadan Mao, Chengwang Lei, and John C Patterson. Unsteady natural convection in a triangular enclosure induced by absorption of radiation–a revisit by improved scaling analysis. *Journal of Fluid Mechanics*, 622:75–102, 2009.

[13] Yadan Mao, Chengwang Lei, and John C Patterson. Unsteady near-shore natural convection induced by surface cooling. *Journal of Fluid Mechanics*, 642:213–233, 2010.

[14] Yadan Mao, Chengwang Lei, and John C Patterson. Unsteady nearshore natural convection induced by constant isothermal surface heating. *Journal of Fluid Mechanics*, 707:342–368, 2012.

[15] Chengwang Lei and John C Patterson. A direct stability analysis of a radiation-induced natural convection boundary layer in a shallow wedge. *Journal of Fluid Mechanics*, 480:161–184, 2003.